



## OPEN ACCESS

## EDITED BY

Tushar Kanti Das,  
Silesian University of Technology, Poland

## REVIEWED BY

Sayan Ganguly,  
University of Waterloo, Canada  
Marcin Jesionek,  
Silesian University of Technology, Poland  
Suman Basak,  
Dyson, United Kingdom

## \*CORRESPONDENCE

Shaoyun Xu,  
✉ xusy1985@126.com

RECEIVED 18 October 2024

ACCEPTED 07 November 2024

PUBLISHED 20 November 2024

## CITATION

Xu S, Tang J and Wang L (2024) Experimental research on the chlorine salt corrosion resistance of alkali activated low-carbon concrete.

*Front. Mater.* 11:1513262.

doi: 10.3389/fmats.2024.1513262

## COPYRIGHT

© 2024 Xu, Tang and Wang. This is an open-access article distributed under the terms of the [Creative Commons Attribution License \(CC BY\)](https://creativecommons.org/licenses/by/4.0/). The use, distribution or reproduction in other forums is permitted, provided the original author(s) and the copyright owner(s) are credited and that the original publication in this journal is cited, in accordance with accepted academic practice. No use, distribution or reproduction is permitted which does not comply with these terms.

# Experimental research on the chlorine salt corrosion resistance of alkali activated low-carbon concrete

Shaoyun Xu<sup>1\*</sup>, Jianzhong Tang<sup>2</sup> and Limin Wang<sup>3</sup>

<sup>1</sup>College of Architectural Engineering, Jiangsu College of Engineering and Technology, Nantong, China, <sup>2</sup>Nantong Langji New Building Materials Co., Ltd., Nantong, China, <sup>3</sup>Department of Civil and Airport Engineering, Nanjing University of Aeronautics and Astronautics, Nanjing, China

This paper presents orthogonal experiments to investigate the effects of sol ratio, content of fly ash and slag, expander and modulus of sodium silicate on the chlorine salt corrosion resistance of alkali activated low-carbon concrete (AALC). The microstructures and product compositions of AALC after chloride ion erosion were further analyzed by Scanning Electron Microscopy (SEM) and X-Ray Diffraction (XRD). The results show that with an increase of sol ratio, the color depth of AALC gradually increases at 28 days, but the growth trend slows down, the difference of unsteady migration coefficient between sol ratio of 0.44 and 0.46 at 28 days is not obvious, and the unsteady migration coefficient increases first and then decreases at 56 days. As the fly ash content increases, the color depth of AALC increases significantly, when the fly ash content is 10%, it increases by 28.92% compared with AALC without fly ash, and when the fly ash content is 20%, it increases by 27.10% compared with that of 10%. With an increase of fly ash content, the unsteady migration coefficient gradually increases at 14, 28 and 56 days, when the fly ash content is 10%, it increases by 60.66% compared with AALC without fly ash, and when the fly ash content is 20%, it increases by 78.57% compared with that of 10%. As the content of expander increases, the color depth of AALC shows a trend of first decreasing and then increasing, the unsteady migration coefficients of 14, 28 and 56 days all increases first and then decreases. As the modulus of sodium silicate ( $M_s$ ) increases, the color depth of AALC at 28 days decreases first and then increases, the unsteady migration coefficients at 14, 28 and 56 days all decreases first and then increases. In the process of sodium chloride solution soaking, the solution enters the internal pores of AALC, and unhydrated slag and fly ash will further react with sodium chloride to generate new hydration product of C-A-S-H. The hydration degree of AALC increases, and the internal structure becomes denser, corresponding to the peak value of hydration product C-S-H gel increases.

## KEYWORDS

alkali excitation, low-carbon concrete, chloride ion penetration, erosion, microstructure

## 1 Introduction

Concrete is widely used due to its high strength and low cost (Montemor et al., 2003). The extensive use of Portland cement has brought inevitable carbon emissions and environmental pollution problems. It not only consumes a large amount of energy and resources, but also accelerates the greenhouse effect of the atmosphere, which is not conducive to the sustainable development of society. In the long run, it is imperative to develop green and low-carbon new building materials. Alkali activated material is a new type of green cementitious material, which is prepared by using silicoaluminate natural minerals or industrial solid waste rich in silicoaluminate as precursors and alkaline activators (Proms et al., 2013). It is not only environmentally friendly with low carbon emission and low pollution, but also has excellent mechanical properties and durability (Bakharev, 2005; Ma et al., 2018). It can be used in concrete instead of cement, which can improve the working performance of concrete, reduce the engineering cost and reduce carbon emissions (Garcipalomo and Jimenez, 2007). It is considered to be the most suitable and promising cement substitute with broad application prospects (Padmakar and Kumar, 2017; Palomo et al., 1999; Fan et al., 2018). Alkali-activated materials can be applied to marine structures and sewer pipes (Yang et al., 2022; Kong et al., 2022), there is a large amount of chloride ion erosion in this kind of environment, which will cause obvious damage to the alkali-excited reinforced concrete structure.

Scholars around the world have done a lot of research on the chlorine salt corrosion resistance of alkali-activated cementitious materials concrete. Kumar et al. found that in the marine environment, alkali activated fly ash concrete exhibits superior resistance to chloride ion attack compared with Portland cement concrete (Reddy et al., 2013; Kumar and Ramujee, 2016). Gunasekara et al. found through their research that the matrix will form N-A-S-H and C-A-S-H gel coexistence when fly ash is added to the alkali slag system. Under the appropriate ratio, the two gel will be crosslinked to jointly improve the chloride ion corrosion resistance of the matrix, it can effectively make alkali-activated concrete reduce the corrosion rate of steel bars (Gunasekara et al., 2019). Ma et al. evaluated the chloride ion diffusion coefficient of alkali activated slag concrete based on the NT Build 443 standard and found that the chloride ion diffusion rate of alkali activated slag concrete is approximately one-third that of ordinary cement concrete (Ma et al., 2016). Adam studied the chloride resistance of alkali-activated slag concrete and alkali-activated fly ash concrete by accelerated simulation test in the laboratory. The RCP results showed that the charge passing rate and conductivity of the two alkali-activated concrete are higher than that of ordinary cement concrete (Adam, 2009). Tennakoon found that the chloride diffusion coefficient of alkali-activated fly ash-slag composite concrete is obviously lower than that of ordinary cement concrete, and the diffusion coefficient of chloride ion gradually decreases with the increase of slag content (Tennakoon et al., 2017). The ability of alkali activated composite system concrete to resist chloride ion penetration increases with time, compared with Portland cement concrete, alkali activated concrete has a denser pore structure, more stable chemical properties of hydration products, and stronger resistance to chloride ion erosion (Mangat and Ojedokun, 2018; Ravikumar

and Neithalath, 2013). Water-cement ratio is the most critical factor for the performance of ordinary portland cement, and it also plays an important role in alkali-activated material system. A large number of experiments have shown that increasing the water-cement ratio of activator will reduce the chloride ion corrosion resistance of alkali-activated concrete (Zhu et al., 2014; Zhang et al., 2020). Mangat et al. found that the modulus of silicate in the activator also has an influence on the properties of alkali-activated concrete, and thought that higher modulus usually makes the pore structure of alkali-activated material system more dense, and then shows more excellent chloride ion resistance (Mangat and Ojedokun, 2019). Shi Caijun et al. found that alkali-activated concrete prepared by alkali metal activator of hydroxide has poor pore structure, since there is no silicon-containing substance in alkali metal activator solution of hydroxide to promote gel formation, so its chloride ion resistance is lower than that of silicate activator (Hu et al., 2019). Jena et al. tried to mix 5% silica fume as an external admixture in the alkali-activated material system, and the result showed that silica fume could effectively enhance the chloride ion corrosion resistance of alkali-activated materials (Jena et al., 2019). Khater et al. pointed out that it is unnecessary or even harmful to add excessive silica fume. They verified this statement through experiments. When the silica fume content is more than 7%, caking will be formed in a small area in the alkali-activated matrix, which will hinder the formation of gel and lead to the decline of performance (Khater, 2013). Yoon found that adding a small amount of MgO (<5%) to the alkali activated material system can improve its resistance to chloride ion corrosion. However, excessive MgO content may also lead to the opposite result, in their opinion, excessive MgO may lead to adverse effects on matrix pore size, continuity and chemical composition of pore solution (Yoon et al., 2018). It is also reported in the literature that adding magnesium-containing additives can improve the chloride ion binding ability of the matrix, thus reducing the chloride ion transmission rate (Ke et al., 2017). Ma Q et al. have evaluated alkali excited concrete and Portland cement concrete by resistivity, unstable chloride ion diffusion rate, corrosion initiation time, corrosion rate and pore solution chemistry. It has been found that alkali activated concrete shows stronger resistance to chloride ion corrosion (Ma et al., 2015). Ravikumar D found that the electric flux of alkali slag geopolymer concrete excited by sodium silicate solid powder is less than that of geopolymer concrete excited by water glass. First, the conductivity of its pore solution is less than that of concrete excited by water glass, because the sodium silicate solid powder cannot be completely dissolved at room temperature. Second, the pore structure of concrete excited by different kinds of activators is also different (Ravikumar and Neithalath, 2013). Kupwade-Patil K et al. have prepared alkali-activated concrete with F-grade fly ash and C-grade fly ash respectively to research its chlorine resistance. The results have shown that the alkali activated concrete prepared with C-grade fly ash (12.93% CaO) has low chlorine resistance (Kupwade-Patil and Allouche, 2013). The fineness of fly ash will also affect the compressive strength and microstructure. The finer the fineness of fly ash particles, the smaller the gap between particles, which can lead to the decrease of the overall porosity and pore size of alkali activated materials, and then improve the strength and chlorine resistance of the matrix (Somna et al., 2011).

TABLE 1 Chemical composition of slag and fly ash (%).

Materials	CaO	SiO <sub>2</sub>	Al <sub>2</sub> O <sub>3</sub>	MgO	SO <sub>3</sub>	TiO <sub>2</sub>	Fe <sub>2</sub> O <sub>3</sub>	MnO	Others
Slag	43.26	29.32	16.78	7.04	1.71	0.88	0.55	0.46	-
Fly ash	5.65	53.21	32.36	1.58	2.23	-	2.87	-	2.1

TABLE 2 Performance of water glass.

Target	Modulus	Baume degree	Density	SiO <sub>2</sub> (%)	Na <sub>2</sub> O(%)	Insoluble (%)	Iron content (%)
Value	3.1–3.4	39.2–40.2	1.368–1.394	≥26	≥8.2	≤0.2	≤0.02

The preliminary research on the durability of alkali activated concrete mainly focuses on acid resistance, freeze-thaw resistance, carbonation, and other aspects (Luhar et al., 2019; Parthiban and Saravana Raja Mohan, 2017; Ban et al., 2017), and the research results on its resistance to chloride ion penetration are quite scattered. In order to correctly evaluate the ability of alkali-activated concrete to resist steel corrosion, it is necessary to study its chloride ion resistance. Such research will also promote the application and development of alkali activated cementitious materials to a certain extent, which has practical significance. At the same time, we need to pay attention to environmental protection (Kanti Das et al., 2024; Kanti Das et al., 2023).

At present, there are few studies on the effects of fly ash slag composite ratio, sol ratio, modulus of sodium silicate and expander agent on the chloride ion resistance of AALC. In this paper, AALC was prepared by orthogonal experiments, and the effects of composite ratio of fly ash and slag, sol ratio, modulus of sodium silicate and expander on chloride ion penetration resistance at different ages were researched. Meanwhile, Scanning Electron Microscopy (SEM) and X-Ray Diffraction (XRD) were used to further analyze and compare the microstructure of AALC with different proportions.

## 2 Experiment materials and methods

### 2.1 Materials

Grade I fly ash and slag were produced in Nanjing, with chemical compositions shown in Table 1. Their performance indicators met the requirements of the GB/T18046-2000 and GB/T1596-2005 Chinese standards, respectively. Sodium silicate was produced in Shanghai with a modulus (Ms) of 3.24 and Na<sub>2</sub>O and SiO<sub>2</sub> contents of 8.73 wt% and 27.45 wt%, respectively. Specific indicators are shown in Table 2. Ms was adjusted by adding NaOH. Analytically pure NaOH, i.e., was produced in Shanghai, the main component content was greater than 99%. River sand with fineness modulus of 2.58 and basalt gravel with particle size of 5–20 mm were used. The performance indicators of expander, produced in Nanjing, met the requirements of the GB50119-2013 Chinese standards. The performance indicators are shown in Table 3.

### 2.2 Specimens preparation and testing programs

In order to research the effect of sol ratio, fly ash content, expander content and Ms on chloride ion penetration resistance of AALC, the L<sub>9</sub> (3<sup>4</sup>) orthogonal test was adopted. Table 4 lists orthogonal test factor level, Table 5 lists AALC mix ratio.

The concrete specimen with a diameter of 100 mm and a height of 50 mm was used to test the unsteady migration coefficient by the RCM (Rapid Chloride Migration) test method, in accordance with the relevant test methods in GB/T 50082-2009, the schematic diagram is shown in Figure 1. The concrete specimen was split along the axial direction by the press after the completion of the chloride ion migration coefficient test, AgNO<sub>3</sub> solution with a concentration of 0.1 mol/L was immediately sprayed on the fault, and then the color depth was measured, accurate to 0.1 mm.

The unsteady migration coefficient was calculated using Equation 1:

$$D_{RCM} = \frac{0.0239(273 + T)L_h}{(U-2)t} \left( x_d - 0.0238 \sqrt{\frac{(273 + T)L * x_d}{U-2}} \right) \quad (1)$$

Where DRCM is unsteady migration coefficient at different ages, accurate to 0.1 × 10<sup>-12</sup> m<sup>2</sup>/s, t is the test duration, in h, U is the absolute value of voltage, in V, T is the average of the initial and final temperatures of the anode solution, in °C, x<sub>d</sub> is the average depth of chloride ion penetration, accurate to 0.1 mm, L<sub>h</sub> is the Specimen thickness, accurate to 0.1 mm.

The 5 mm × 5 mm × 5 mm samples that had been cured for 28 days were soaked in anhydrous ethanol for 3 days, and the samples were taken out and dried in a vacuum at 60°C for 48 h. The JSM-6510 high resolution scanning electron microscope was used for SEM scanning analysis.

The samples were taken from absolute ethanol that had been cured for 28 days, dried in the vacuum at 60°C for 24 h, partially ground to powder and sieved through 80 μm sieve, D8 advance X-ray diffractometer was used for XRD analysis under the scanning range of 10° to 80° at a scanning rate of 0.30s/step, step size = 0.02°. Some samples were analyzed by mercury intrusion, and the test was performed by Auto Pore IV 9510 mercury injection meter produced by Micromeritics Instrument Corporation (Norcross, GA, United States).

TABLE 3 Properties and composition of calcium oxide expansion agent.

CaO	Component (%)				Setting time (min)	
	Sieving Residue	Humidity	Alkali Content	Cl <sup>-</sup>	Initial Set	Final Set
≥98	≤0.50	≤0.40	≤0.20	≤0.03	165	350

TABLE 4 Orthogonal test factor level.

NO.	Fly ash content (FA%)	Sol ratio (S/C)	Modulus (Ms)	Expander (EA%)
1	0%	0.42	1.2	0%
2	10%	0.44	1.4	2%
3	20%	0.46	1.6	4%

TABLE 5 AALC mix ratio (kg/m<sup>3</sup>).

NO.	Fly ash (kg/m <sup>3</sup> )	Slag (kg/m <sup>3</sup> )	Alkali solution (kg/m <sup>3</sup> )	Expander (kg/m <sup>3</sup> )	Sand (kg/m <sup>3</sup> )	Gravel (kg/m <sup>3</sup> )
L1	0	400	168	0	716	1,074
L2	0	400	176	8	716	1,074
L3	0	400	184	16	716	1,074
L4	40	360	168	16	716	1,074
L5	40	360	176	0	716	1,074
L6	40	360	184	8	716	1,074
L7	80	320	168	8	716	1,074
L8	80	320	176	16	716	1,074
L9	80	320	184	0	716	1,074

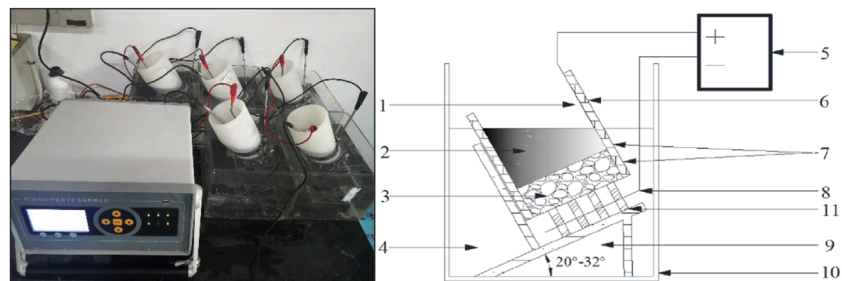


FIGURE 1 Schematic diagram of RCM test 1-anode plate; 2-anodic solution; 3-concrete specimen; 4-cathodic solution; 5-DC regulated power supply; 6-silicone rubber sleeve; 7-hoop; 8-negative plate; 9-support; 10-cathodic test tank; 11-brace .

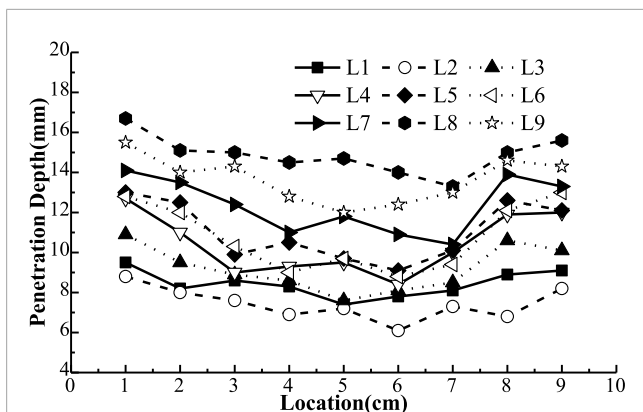


FIGURE 2 The 28 days penetration depth of AALC.

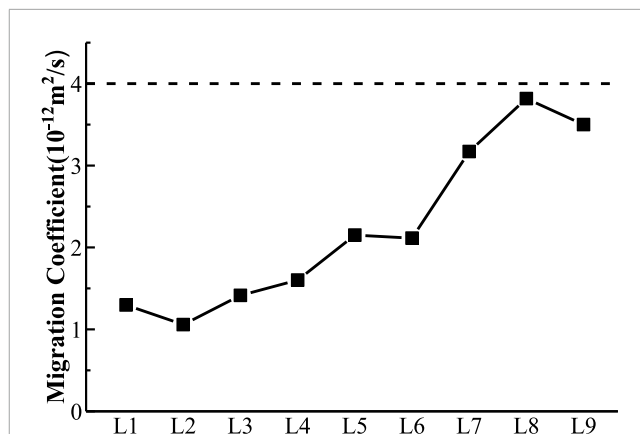


FIGURE 4 Unsteady migration coefficient of concrete.

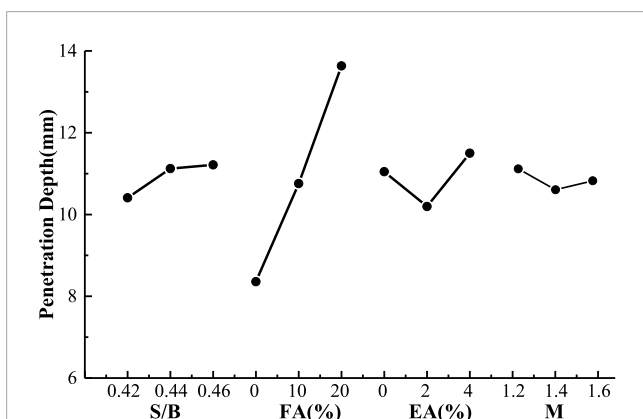


FIGURE 3 The influence of different factors on 28 days color depth.

### 3 Results and discussion

#### 3.1 Penetration depth of chloride ion

The chloride ion penetration depth of L1~L9 AALC at 28 days is shown in Figure 2. In the figure, it can be seen that the color boundary of AALC after chloride ion penetration is defined by the colored area below the line (ion penetration area) and the uncolored area above the line (non-ion penetration area).

Figure 2 shows that the average penetration depth of chloride ions in L1~L9 AALC was less than 15 mm, and the lowest penetration depth in L2 was only 7 mm. The order of color development depth of AALC at 28 days was L2 < L1 < L3 < L4 < L6 < L5 < L7 < L9 < L8.

The effects of sol ratio, fly ash content, expander content and Ms on the color depth of AALC at 28 days are shown in Figure 3.

Figure 3 shows that with the increase of sol ratio, the color depth of AALC increased gradually at 28 days. When the sol ratio was 0.44 and 0.46, color depth was increased by 6.87% and 7.76% compared with a 0.40 sol ratio, respectively. As the sol ratio increases, the reaction rate of the composite system decreases, and the speed of forming C-S-H gel slows down, so the structure is looser. At the

same time, with the increase of sol ratio, the free water in the system increases, the pores left after evaporation from the system increase, resulting in an increase in porosity and a looser structure. Therefore, as the sol ratio increases, the number of pores in the composite system concrete increases, making it easier for chloride ions to enter the system and the color depth increases at 28 days.

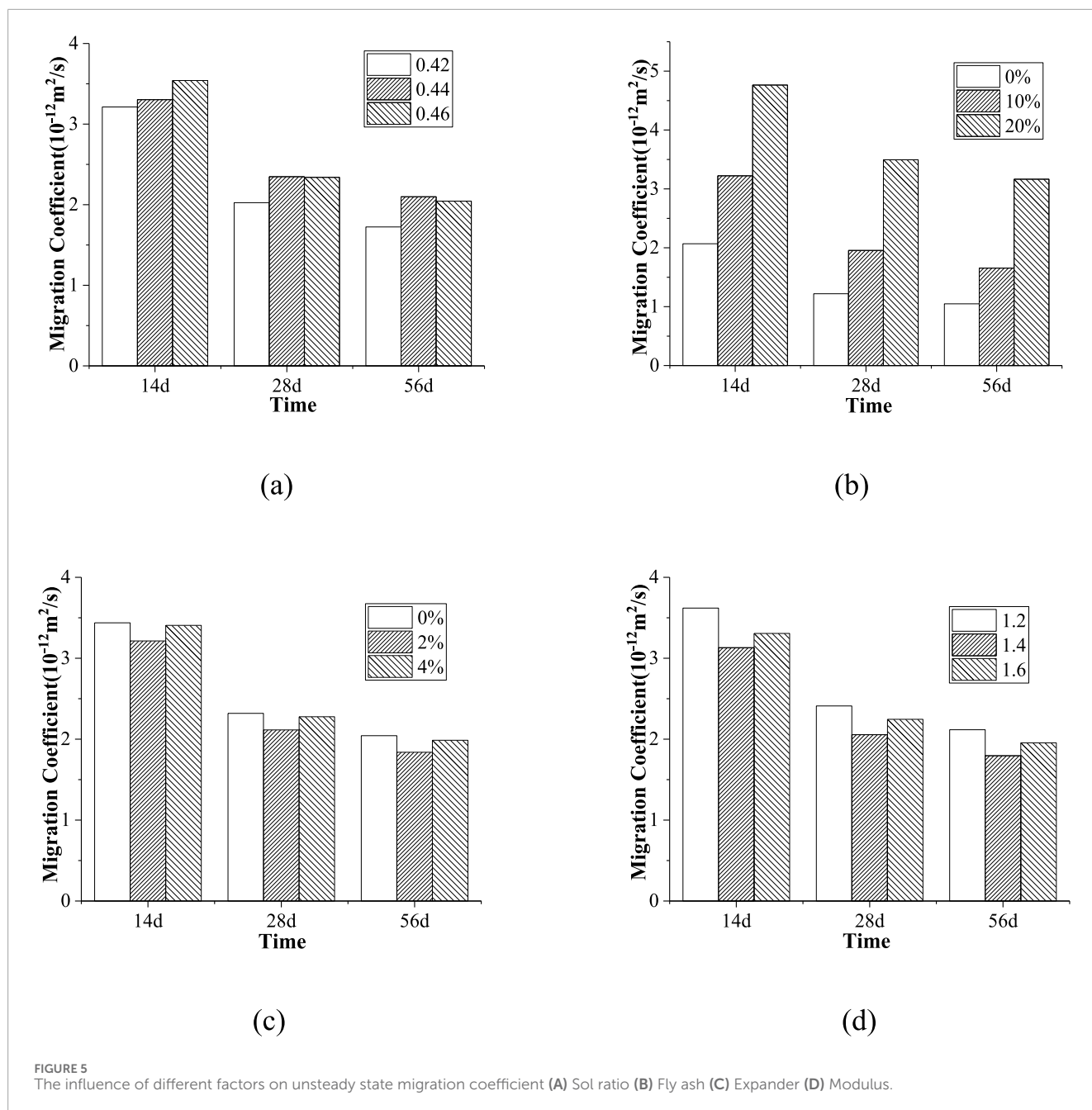
As illustrated in Figure 3, as the content of fly ash increased, the color depth of AALC increased significantly at 28 days. When the fly ash content was 10% and 20%, color depth was increased by 28.72% and 63.16% compared with that without fly ash, respectively. It can be seen that AALC without fly ash underwent smallest color depth at 28 days. This is because the internal structure without fly ash is more complete, making it more difficult for chloride ions to penetrate.

As shown in Figure 3, with the increase of the content of expander, the color depth of AALC showed a decreasing and then an increasing trend at 28 days. Due to the addition of expander, ettringite crystals are generated in the composite system, and AALC expands under the action of crystallization pressure, the pores decrease, the density increases, and the depth of chloride ion penetration first decreases. However, with the further increase of the content, the water consumed by expander increases, which affects the fluidity and reduces the performance of concrete, so the color depth increases again.

Figure 3 shows that as the Ms increased, the color depth of AALC showed a decreasing and then an increasing trend at 28 days. It shows that when the Ms increases in a certain range, the structure of AALC becomes denser, and the porosity decreases, so the penetration depth of chloride ions decreases. However, when the Ms exceeds a certain range, the generation of reaction products is inhibited, the reaction rate and the density decrease, the pores increase, and chloride ions are more likely to enter the interior of AALC.

#### 3.2 Unsteady migration coefficient

The unsteady migration coefficient of AALC is obtained after processing the test data according to Formula 1. The test results are shown in Figure 4. As shown in the figure, the unsteady state



migration coefficients of L1 to L9 were all less than  $4.0 \times 10^{-12}$  m<sup>2</sup>/s. This indicates that AALC has excellent resistance to chloride ion penetration. According to the test results, the unsteady migration coefficients of chloride ions in L1~L9 at 28 days were ranked as follows: L2 < L1 < L3 < L4 < L6 < L5 < L7 < L9 < L8. The unsteady migration coefficient of chloride ion in group L2 was the smallest at 28 days, indicating the best resistance to chloride ion transport and the lowest chloride ion transport rate. In the same time period, the amount of chloride ion penetrating into the L2 was the least.

The effects of sol ratio, fly ash content,  $M_s$  and expander content on the unsteady state migration coefficient of AALC at different ages are shown in Figure 5.

Figure 5A shows that as the sol ratio increased, the unsteady migration coefficient of AALC increased at 14 and 28 days. However, the difference of unsteady migration coefficient between sol ratio of 0.44 and 0.46 was not obvious at 28 days, while the unsteady migration coefficient of AALC showed an increasing and then a decreasing trend at 56 days with the increase of sol ratio. This is mainly because with the increase of sol ratio, the free water increases, then the pores caused by the evaporation of free water increase. On the other hand, the excess water will reduce the cohesive force between aggregate and slurry, resulting in micro-cracks, the migration rate of chloride ions increases, so the permeability of chloride ions increases. As time goes on, the hydration of the cementitious material becomes

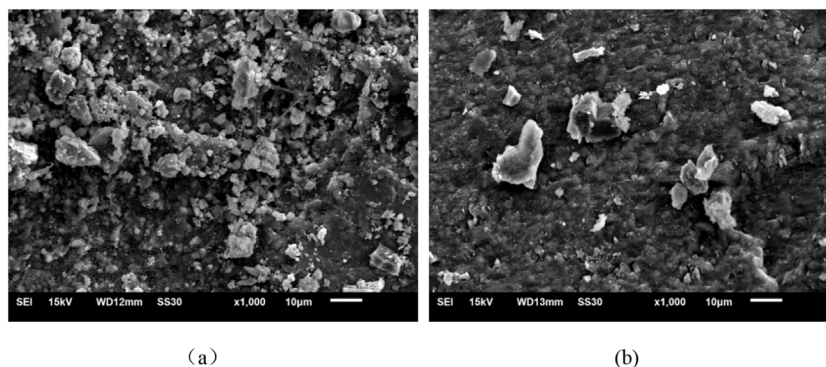


FIGURE 6 SEM image after ion erosion (A) L1 (B) L4.

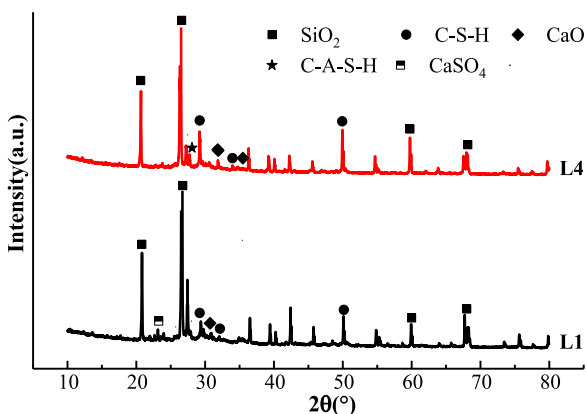


FIGURE 7 XRD spectrum after ion erosion.

more complete, and the ability to resist chloride ion penetration is enhanced.

As illustrated in Figure 5B, as the content of fly ash increased, the unsteady migration coefficient of AALC gradually increased at 14, 28 and 56 days. When the fly ash content was 10% and 20%, the unsteady migration coefficient was increased by 60.26% and 186.53% compared with that without fly ash at 28 days, respectively. It can be seen that the addition of fly ash increases the chloride ion permeability of AALC. This is mainly because the addition of fly ash leads to the decrease of system activity and CaO content, and the hydration products generated by fly ash under excitation have high porosity, while the hydration products generated by slag under excitation have low porosity, so the migration speed of chloride ions is accelerated and the chloride ion penetration resistance is reduced after adding fly ash.

As shown in Figure 5C, as the content of expander was increased, the unsteady migration coefficient of AALC showed a decreasing and then an increasing trend at 14, 28 and 56 days. It shows that the chloride ion penetration resistance first increased and then decreased. The addition of expander is helpful to expand the

interior of the structure, improve the pore structure, reduce the porosity and enhance the resistance to chloride ion penetration. On the other hand, increasing the content of expander will consume a lot of water, reduce the fluidity of the slurry, it will affect the chloride ion permeability of AALC, so the addition of expander has a dual effect on the chloride ion permeability resistance of AALC.

Figure 5D shows that with the increase of  $M_s$ , the unsteady migration coefficient of AALC showed a decreasing and then an increasing trend at 14, 28 and 56 days. When the  $M_s$  was 1.4, the unsteady migration coefficient was decreased by 14.73% compared with a 1.2  $M_s$  at 28 days. When the  $M_s$  was 1.6, the unsteady migration coefficient was increased by 9.26% compared with a 1.4  $M_s$  at 28 days. The results show that the increase of  $M_s$  can enhance the chloride ion penetration resistance of AALC. Increasing  $M_s$  under the condition of constant alkali content can increase the hydration products, improve the pore structure, reduce porosity, and enhance resistance to chloride ion penetration. However, with the continuous increase of  $M_s$ , the alkali content in the system decreases, leading to a weakened alkaline reaction environment and further reducing the reaction rate, resulting in an increase in porosity. As a result, the chloride ion penetration resistance decreases and the unsteady migration coefficient increases.

### 3.3 SEM analysis

The L1 and L4 samples, permeated by chloride ions for 28 days, were selected for SEM analysis.

As shown in Figure 6, during the soaking process in sodium chloride solution, the solution penetrated into the internal pores of AALC. The unhydrated slag and fly ash would further react with sodium chloride to generate new hydration products, either clustering into a mass or presenting as a reticular structure that connects together, so that the hydration degree increased and the internal structure became denser, and some unreacted sodium chloride crystals would be crystallized and filled in the pores of concrete.

### 3.4 XRD analysis

XRD analysis of AALC after chloride ion erosion in L1 and L4 was carried out, and the reaction products after chloride ion erosion were specifically studied.

Figure 7 shows the XRD patterns of L1 and L4. Fly ash particles have a hollow structure and a large internal specific surface area, which makes chloride ions easily adsorbed on its surface, thus slowing down the seepage velocity of chloride ions. At the same time, chloride ions participate in hydration, and the number of C-S-H gel increases, further promoting the hydration reaction of alkali activated low-carbon concrete, then the corresponding peak value of hydration product C-S-H gel would increase, and a new hydration product C-A-S-H gel would be generated.

## 4 Conclusion

Based on experimental research and a theoretical analysis of AALC, the following conclusions were obtained:

- (1) The color depth of chloride ions in AALC at 28 days was less than 15 mm. With the increase of sol ratio and fly ash content, the color depth of AALC at 28 days increased gradually. When the sol ratio was 0.44 and 0.46, color depth was increased by 6.87% and 7.76% compared with a 0.40 sol ratio, respectively. When the fly ash content was 10% and 20%, color depth was increased by 28.72% and 63.16% compared with that without fly ash, respectively. As the content of expander and  $M_s$  increased, the color depth of AALC showed a decreasing and then an increasing trend at 28 days.
- (2) The unsteady migration coefficient of chloride ions in AALC was less than  $4.0 \times 10^{-12} \text{ m}^2/\text{s}$  at 28 days. With the increase of fly ash content, the unsteady migration coefficient of chloride ions in AALC gradually increased at 28 days. When the fly ash content was 10% and 20%, the unsteady migration coefficient was increased by 60.26% and 186.53% compared with that without fly ash at 28 days, respectively. As the sol ratio increased, the unsteady migration coefficient of chloride ions showed an increasing and then a decreasing trend at 56 days. As the content of expander and  $M_s$  increased, the unsteady migration coefficient of chloride ions showed a decreasing and then an increasing trend at 14, 28 and 56 days. When the  $M_s$  was 1.4, the unsteady migration coefficient was decreased by 14.73% compared with a 1.2  $M_s$  at 28 days. When the  $M_s$  was 1.6, the unsteady migration coefficient was increased by 9.26% compared with a 1.4  $M_s$  at 28 days.
- (3) In the process of soaking in sodium chloride solution, the solution penetrated into the internal pores of AALC, and unhydrated slag and fly ash would further react with sodium chloride to generate new hydration products to fill the pores, so the internal structure was more compact. The peak value of C-S-H gel increased, at

the same time, new hydration product C-A-S-H gel was formed.

## Data availability statement

The original contributions presented in the study are included in the article/supplementary material, further inquiries can be directed to the corresponding author.

## Author contributions

SX: Funding acquisition, Investigation, Methodology, Project administration, Writing—original draft. JT: Resources, Visualization, Writing—review and editing. LW: Conceptualization, Data curation, Methodology, Visualization, Writing—review and editing.

## Funding

The author(s) declare that financial support was received for the research, authorship, and/or publication of this article. This work was supported by the Jiangsu Province Construction System Science and Technology Project (2023ZD045), Nantong Social Livelihood Science and Technology Plan Project (MSZ2023108), Jiangsu Province Vice President of Science and Technology Project (FZ20230556), Nantong Basic Science Research and Social Livelihood Science and Technology Plan Project (JCZ2022116), General Project of Basic Science (Natural Science) Research in Colleges and Universities in Jiangsu Province (23KJD170002), Teaching Reform Research Project of Jiangsu College of Engineering and Technology (GYJY202328).

## Conflict of interest

Author JT was employed by Nantong Langji New Building Materials Co., Ltd.

The remaining authors declare that the research was conducted in the absence of any commercial or financial relationships that could be construed as a potential conflict of interest.

## Generative AI statement

The author(s) declare that no Generative AI was used in the creation of this manuscript.

## Publisher's note

All claims expressed in this article are solely those of the authors and do not necessarily represent those of their affiliated organizations, or those of the publisher, the editors and the reviewers. Any product that may be evaluated in this article, or claim that may be made by its manufacturer, is not guaranteed or endorsed by the publisher.

## References

- Adam, A. (2009). *Strength and durability properties of alkali activated slag and fly ash-based geopolymer concrete*. RMIT University.
- Bakharev, T. (2005). Resistance of geopolymer materials to acid attack. *Cem. Concr.* 35 (4), 658–670. doi:10.1016/j.cemconres.2004.06.005
- Ban, C. C., Ken, P. W., and Ramli, M. (2017). Mechanical and durability performance of novel self-activating geopolymer mortars. *Procedia Eng.* 171, 564–571. doi:10.1016/j.proeng.2017.01.374
- Fan, F., Liu, Z., Xu, G., Peng, H., and Cai, C. (2018). Mechanical and thermal properties of fly ash based geopolymers. *Constr. Build. Mater.* 160, 66–81. doi:10.1016/j.conbuildmat.2017.11.023
- Garcipalomo, L. A., and Jimenez, F. (2007). Alkali-aggregate reaction in activated fly ash systems. *Cem. Concr. Res.* 37, 175–183. doi:10.1016/j.cemconres.2006.11.002
- Gunasekara, C., Law, D., Bhuiyan, S., Setunge, S., and Ward, L. (2019). Chloride induced corrosion in different fly ash based geopolymer concretes. *Constr. Build. Mater.* 200 (MAR.10), 502–513. doi:10.1016/j.conbuildmat.2018.12.168
- Hu, X., Shi, C., Shi, Z., and Zhang, L. (2019). Compressive strength, pore structure and chloride transport properties of alkali-activated slag/fly ash mortars. *Cem. Concr. Compos.* 104, 103392. doi:10.1016/j.cemconcomp.2019.103392
- Jena, S., Panigrahi, R., and Sahu, P. (2019). Mechanical and durability properties of fly ash geopolymer concrete with silica fume. *J. Institution Eng. (India) Ser. A* 100 (4), 697–705. doi:10.1007/s40030-019-00400-z
- Kanti Das, T., Basak, S., and Ganguly, S. (2024). 2D nanomaterial for microplastic Removal: a critical review. *Chem. Eng. J.* 492, 152451. doi:10.1016/j.cej.2024.152451
- Kanti Das, T., Jesionek, M., Çelik, Y., and Poater, A. (2023). Catalytic polymer nanocomposites for environmental remediation of wastewater. *Sci. Total Environ.* 901, 165772. doi:10.1016/j.scitotenv.2023.165772
- Ke, X., Bernal, S. A., Hussein, O. H., and Provis, J. L. (2017). Chloride binding and mobility in sodium carbonate-activated slag pastes and mortars. *Mater. Struct.* 50 (6), 252. doi:10.1617/s11527-017-1121-8
- Khater, H. M. (2013). Effect of silica fume on the characterization of the geopolymer materials. *Int. J. Adv. Struct. Eng.* 5 (1), 12. doi:10.1186/2008-6695-5-12
- Kong, L., Zhao, W., Xuan, D., Wang, X., and Liu, Y. (2022). Application potential of alkali-activated concrete for antimicrobial induced corrosion: a review. *Constr. Build. Mater.* 317, 126169. doi:10.1016/j.conbuildmat.2021.126169
- Kumar, S., and Ramujee, K. (2016). Assessment of chloride ion penetration of alkali activated low calcium fly ash based geopolymer concrete. *Key Eng. Mater.* 692, 129–137. doi:10.4028/www.scientific.net/kem.692.129
- Kupwade-Patil, K., and Allouche, E. N. (2013). Examination of chloride-induced corrosion unreinforced geopolymer concretes. *J. Mater. Civ. Eng.* 25 (10), 1465–1476. doi:10.1061/(asce)mt.1943-5533.0000672
- Luhar, S., Cheng, T., Nicolaidis, D., Luhar, I., Pnias, D., and Sakkas, K. (2019). Valorisation of glass wastes for the development of geopolymer composites-Durability, thermal and microstructural properties: a review. *Constr. Build. Mater.* 222, 673–687. doi:10.1016/j.conbuildmat.2019.06.169
- Ma, C.-K., Awang, A. Z., and Omar, W. (2018). Structural and material performance of geopolymer concrete: a review. *Constr. Build. Mater.* 186, 90–102. doi:10.1016/j.conbuildmat.2018.07.111
- Ma, Q., Nanukuttan, S. V., Basheer, P. a. M., and BaiY Yang, C. (2015). Chloride transport and the resulting corrosion of steel bars in alkali activated slag concretes. *Mater. Struct.* 49 (9), 3663–3677. doi:10.1617/s11527-015-0747-7
- Mangat, P. S., and Ojedokun, O. O. (2018). Influence of curing on pore properties and strength of alkali activated mortars. *Constr. Build. Mater.* 188, 337–348. doi:10.1016/j.conbuildmat.2018.07.180
- Mangat, P. S., and Ojedokun, O. O. (2019). Title: bound chloride ingress in alkali activated concrete. *Constr. Build. Mater.* 212 (JUL.10), 375–387. doi:10.1016/j.conbuildmat.2019.03.302
- Ma, Q., Nanukuttan, S. V., Basheer, P. A. M., Bai, Y., and Yang, C. (2016). Chloride transport and the resulting corrosion of steel bars in alkali activated slag concretes. *Mater. Struct.* 49 (9), 3663–3677. doi:10.1617/s11527-015-0747-7
- Montemor, M. F., Simoes, A. M. P., and Ferreira, M. G. S. (2003). Chloride-induced corrosion on reinforcing steel: from the fundamentals to the monitoring techniques. *Cem. Concr.* 25 (4), 491–502. doi:10.1016/s0958-9465(02)00089-6
- Padmakar, K. C., and Kumar, B. S. C. (2017). An experimental study on metakaolin and GGBS based geopolymer concrete. *Int. J. Engineering&Technology* 8 (1), 544–557. doi:10.21817/ijet/2017/v9i1/170902311
- Palomo, A., Grutzeck, M. W., and Blanco, M. T. (1999). Alkali-activated fly ashes: a cement for the future. *Cem. Concr. Res.* 29 (8), 1323–1329. doi:10.1016/s0008-8846(98)00243-9
- Parthiban, K., and Saravana Raja Mohan, K. (2017). Influence of recycled concrete aggregates on the engineering and durability properties of alkali activated slag concrete. *Constr. Build. Mater.* 133, 65–72. doi:10.1016/j.conbuildmat.2016.12.050
- Proms, J. L., Hajimohammadi, A., White, C. E., Bernal, S. A., Myers, R. J., Winarski, R. P., et al. (2013). Nanostructural characterization of geopolymers by advanced beamline techniques. *Cem. Concr. Compos.* 36, 56–64. doi:10.1016/j.cemconcomp.2012.07.003
- Ravikumar, D., and Neithalath, N. (2013). Electrically induced chloride ion transport in alkali activated slag concretes and the influence of microstructure. *Cem. Concr. Res.* 47, 31–42. doi:10.1016/j.cemconres.2013.01.007
- Reddy, D. V., Edouard, J.-B., and Sobhan, K. (2013). Durability of fly ash-based geopolymer structural concrete in the marine environment. *J. Mater. Civ. Eng.* 25 (6), 781–787. doi:10.1061/(asce)mt.1943-5533.0000632
- Somna, K., Jaturapitakkul, C., Kajitvichyanukul, P., and Chindaprasirt, P. (2011). Naoh-activated groundfly ash geopolymer cured at ambient temperature. *Fuel* 90 (6), 2118–2124. doi:10.1016/j.fuel.2011.01.018
- Tennakoon, C., Shayan, A., Sanjayan, J. G., and Xu, A. (2017). Chloride ingress and steel corrosion in geopolymer concrete based on long term tests. *Mater. and Des.* 116, 287–299. doi:10.1016/j.matdes.2016.12.030
- Yang, G., Zhao, J., and Wang, Y. (2022). Durability properties of sustainable alkali-activated cementitious materials as marine engineering material: a review. *Mater. Today Sustain.* 17, 100099. doi:10.1016/j.mtsust.2021.100099
- Yoon, H. N., Park, S. M., and Lee, H. K. (2018). Effect of mgo on chloride penetration resistance of alkali-activated binder. *Construction&Building Mater.* 178 (JUL.30), 584–592. doi:10.1016/j.conbuildmat.2018.05.156
- Zhang, J., Ma, Y., Zheng, J., Hu, J., Fu, J., Zhang, Z., et al. (2020). Chloride diffusion in alkali-activated fly ash/slag concretes: role of slag content, water/binder ratio, alkali content and sand-aggregate ratio. *Constr. Build. Mater.*, 261. doi:10.1016/j.conbuildmat.2020.119940
- Zhu, H., Zhang, Z., Zhu, Y., and Tian, L. (2014). Durability of alkali-activated fly ash concrete: Chloride penetration in pastes and mortars. *Constr. Build. Mater.* 65, 51–59. doi:10.1016/j.conbuildmat.2014.04.110